Impact of melt ponds on Arctic sea ice in past and future climates as simulated by MPI-ESM

Erich Roeckner,[1] Thorsten Mauritsen,[1] Monika Esch,[1] and Renate Brokopf[1]

Received 1 March 2012; revised 26 July 2012; accepted 1 August 2012; published 6 September 2012.

[1] The impact of melt ponds on Arctic sea ice is estimated from model simulations of the historical and future climate. The simulations were performed with and without the effect of melt ponds on sea ice melt, respectively. In the last thirty years of the historical simulations, melt ponds develop predominantly in the continental shelf regions and in the Canadian archipelago. Accordingly, the ice albedo in these regions is systematically smaller than in the no-pond simulations, the sea ice melt is enhanced, and both the ice concentration and ice thickness during the September minimum are reduced. Open ponds decrease the ice albedo, resulting in enhanced ice melt, less sea ice and further pond growth. This positive feedback entails a more realistic representation of the seasonal cycle of Northern Hemisphere sea ice area. Under the premise that the observed decline of Arctic sea ice over the period of modern satellite observations is mainly externally driven and, therefore, potentially predictable, both model versions underestimate the decline in Arctic sea ice. This presupposition, however, is challenged by our model simulations which show a distinct modulation of the downward Arctic sea ice trends by multidecadal variability. At longer time scales, an impact of pond activation on Arctic sea ice trends is more evident: In the Representative Concentration Pathway scenario RCP45, the September sea ice is projected to vanish by the end of the 21st century. In the active-pond simulation, this happens up to two decades earlier than in the no-pond simulations.

Citation: Roeckner, E., T. Mauritsen, M. Esch, and R. Brokopf (2012), Impact of melt ponds on Arctic sea ice in past and future climates as simulated by MPI-ESM, *J. Adv. Model. Earth Syst., 4*, M00A02, doi:10.1029/2012MS000157.

1. Introduction

[2] Over the period of modern satellite observations, 1979–2006, the Arctic sea ice extent, at the end of the summer melt season in September, has declined at an average rate of −9.1%/decade [*Stroeve et al.*, 2007]. Just slightly smaller (−7.8%/decade) is the trend derived from a blended dataset spanning a longer period, 1953–2006. In each of the following five years the mean September ice extent was smaller than in any of the previous years so that the downward trend, 1979–2011, has meanwhile accelerated to −12.0%/decade (based on the monthly NSIDC index, http://nsidc.org/data/seaice_index/). If this multi-decadal decline in Arctic sea ice extent were caused by the observed changes in carbon dioxide and other atmospheric constituents, climate models should in principle be able to reproduce the observed trend. In fact, all model simulations done in the context of the Intergovernmental Panel of Climate Change Fourth Assessment Report (IPCC AR4) show a downward trend, but the decline over the full period of observations, 1953–2006, is severely underestimated in all simulations, and only few models are able to approximately capture the observed trend during the satellite era [*Stroeve et al.*, 2007]. However, these "most realistic" models overestimate the global temperature trend in the 20th century so that the sensitivity ($\Delta SIE/\Delta T$) of the Arctic sea ice extent (SIE) to global warming (ΔT) appears to be underestimated by all of the models under investigation [*Winton*, 2011]. Hence, a lack of external forcing and global warming can be excluded as potential contributors to the inability of climate models to capture the observed multi-decadal decline in Arctic sea ice extent. These apparent model deficiencies are worrying because the simulated future trends might be underestimated as well, so that the Arctic Ocean could be ice free earlier than the models suggest [*Boé et al.*, 2009a].

[3] Several explanations have been put forward to explain the shortcomings of the models. For example, natural variability in atmospheric circulation patterns, such as the Northern Annual Mode (NAM), very likely caused a thinning of the Arctic ice during an extremely positive NAM phase, 1989–1995, through export of thick multiyear ice to the Atlantic via Fram Strait, followed by a strong decline in sea ice extent as thin ice is more susceptible to warming than thick ice [*Rigor and Wallace*, 2004; *Maslanik et al.*, 2007]. Climate

[1]Max Planck Institute for Meteorology, Hamburg, Germany.

1942-2466/12/2012MS000157

models can, however, reproduce only the forced component of climate change and are principally unable to reproduce the temporal sequence of extreme events. The potential significance of the NAM history for Arctic sea ice trends can only be estimated from hindcast simulations with ocean/sea ice models forced by atmospheric observations. Alternative explanations are related to an underestimation of the positive ice albedo feedback [*Flanner et al.*, 2011], overestimation of the negative longwave feedback [*Boé et al.*, 2009b] or to the rather crude representation of sea ice processes [*Rampal et al.*, 2011]. In most climate models, the ice is represented by one layer only, and a parameterization of the sub-grid scale ice thickness distribution is generally missing. In fact, the models performing best in terms of sea ice trends include the most detailed representation of sea ice processes [*Stroeve et al.*, 2007].

[4] In this study, we investigate to what extent the representation of melt ponds may strengthen the ice albedo feedback. In the Arctic, during late spring and summer, solar radiation melts the snow and the upper surface of the ice. This produces meltwater which partly drains into the ocean and partly transforms into melt ponds on the ice. These melt ponds substantially reduce the ice albedo so that the melt rate beneath ponds is two to three times more rapid than that of bare ice [*Fetterer and Untersteiner*, 1998]. This effect is illustrated in Figure 1 which shows the impact of melt ponds on sea ice thickness as measured in August 2007 in the Central Arctic (D. Notz, personal communication, 2011). In this example, the ice below the pond is about 70 cm thinner than next to the pond. Melt ponds have been observed during field experiments, along cruise tracks, from the air, and from space [e.g., *Fetterer and Untersteiner*, 1998; *Perovich et al.*, 2002a, 2002b, 2009; *Sankelo et al.*, 2010; *Tschudi et al.*, 2001, 2008; *Tucker et al.*, 1999; *Yackel et al.*, 2000]. These studies indicate melt pond fractions of up to 80%, depending on the surface roughness, snow cover, ice type, time of year and location. In addition, these studies show that melt ponds on first year ice (FYI) are shallow but cover a larger area than melt ponds on rough multiyear ice (MYI) which form in depressions, and tend to be smaller, deeper and more numerous. These results are confirmed in a recent comprehensive study on melt pond evolution by *Polashenski et al.* [2012] who emphasize the importance of pond drainage by vertical percolation and horizontal meltwater transport to macroscopic flaws at different stages of the seasonal pond evolution.

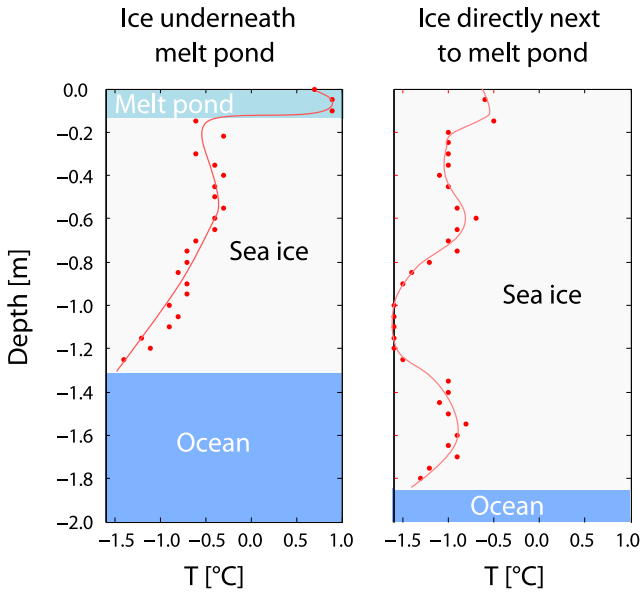

Figure 1. Measurements of temperature, pond depth and sea ice thickness taken during August 2007 on a relatively homogeneous multiyear ice floe at 81°N, 15°E (D. Notz, personal communication, 2011).

[5] In most current climate models, the effect of melt ponds on ice albedo is indirectly taken into account by lowering the ice albedo to a specified value when the ice temperature reaches the melting point. The first attempt to use a simple melt pond model for parameterizing the ice albedo in a coupled model was done by *Pedersen et al.* [2009]. More recently, *Holland et al.* [2012] used a similar scheme in CCSM4. In this study, we follow the approach of *Pedersen et al.* [2009] using distinct parameterizations of fractional pond coverage for FYI and MYI, respectively. The transition of MYI to FYI observed in recent years [*Belchansky et al.*, 2005; *Maslanik et al.*, 2011; *Nghiem et al.*, 2007] leaves the younger and thinner ice pack more vulnerable to summer melt because less energy is needed to melt the ice. Moreover, the ice albedo feedback might be enhanced because the melt pond coverage on FYI, according to both observations and our parameterization, is generally larger than on MYI. As the climate warms, FYI is expected to gradually increase with time, at the expense of MYI, causing melt pond coverage to increase and ice albedo to decrease, thereby possibly enhancing the decline in sea ice extent at the end of the melt season in September. The relevance of this mechanism is tested in simulations of the past and future climate with and without a representation of melt ponds, respectively.

[6] Section 2 gives a short description of the model and the experiments. In sections 2.1 and 2.2, the key elements of the melt pond scheme are described together with its impact on sea ice albedo and sea ice melt. Section 2.3 gives a brief overview of the model and the experiments used in this study. The results are presented in section 3. Spatial distributions of melt ponds, ice albedo, and ice melt are shown in section 3.1, followed by a discussion of basic mechanisms contributing to the decline in surface albedo and sea ice in section 3.2. The changing patterns in sea ice cover and sea ice thickness throughout the 20th and 21st centuries are shown in section 3.3, and trends in Arctic sea ice together with its sensitivity to global warming are discussed in section 3.4. The main conclusions are presented in section 4.

2. Model and Experiments

[7] The coupled model used in this study, MPI-ESM-LR (M. Giorgetta et al., manuscript in preparation, 2012), is based on its predecessor ECHAM5/MPI-OM [*Jungclaus et al.*, 2006]. The ocean and sea ice components

[*Marsland et al.*, 2003] remained largely unchanged. The sea ice dynamics is based on the viscous-plastic rheology developed by *Hibler* [1979]. The thermodynamics relates changes in sea ice thickness to a balance of radiative, turbulent, and oceanic heat fluxes. A subgrid-scale ice thickness distribution is not taken into account, i.e., the sea ice in a grid cell is represented by a single slab of ice defined by its compactness and thickness. The effect of snow accumulation on sea ice is included, along with snow–ice transformation when the snow/ice interface sinks below sea level because of snow loading. The effect of ice formation and melting is accounted for assuming a sea ice salinity of 5 psu. As new ice is formed it is not readily known if the new ice primarily acts to thicken the existing ice, or if it mainly increases the fraction of the grid cell that is ice covered. Likewise, as the ice melts, it is not known if it does so from the top and bottom, or from the sides. In MPI-ESM-LR, the geometry of melting and freezing processes is controlled by two non-dimensional parameters, c_{melt} and c_{freeze}, which can be varied between zero and one. As shown by *Mauritsen et al.* [2012], a change in c_{melt} has a small impact on the Arctic sea ice area in the melt season but no impact in the other seasons nor on the sea ice volume. In contrast, a change in c_{freeze} has a significant effect on the sea ice volume but hardly any impact on the sea ice area. Increasing the "leadclose" parameter c_{freeze}, for example, permits more open ocean to exist during freeze-up which enhances the ocean heat loss to the atmosphere and thereby allows more sea ice to form. This is because even a thin layer of ice is effective in insulating the upper ocean, thereby reducing heat loss and inhibiting further sea ice formation. Even though the process is only effective in fall and early winter, the signature is seen in the ice volume throughout the year, while there is almost no impact on the sea ice area.

[8] The ECHAM5 atmosphere component has been replaced by ECHAM6 (B. Stephens et al., manuscript in preparation, 2012). The changes include a new shortwave radiation scheme, revised cloud optical properties, updated ozone and aerosol climatologies, convection trigger depending on subgrid-scale variability of near-surface virtual potential temperature, revised albedo of water, snow, and sea ice, interactive vegetation, coupling to carbon cycle, and a representation of the middle atmosphere. Except for the higher vertical resolution in the atmosphere (47 layers instead of 31), the resolution of the coupled model remained as in ECHAM5/MPI-OM (T63L47 / 1.5°L40). The processes relevant for this study are detailed below.

2.1. Sea Ice Albedo and Melt Pond Evolution

[9] The scheme is based on the proposal of *Pedersen et al.* [2009], and takes into account separate albedos for snow (α_s), bare ice (α_b), and melt ponds (α_p). The mean ice albedo is defined as

$$\alpha_{ice} = f_s\alpha_s + f_b\alpha_b + f_p\alpha_p \quad (1)$$

where $f_s+f_b+f_p=1$ are the respective fractions of snow, bare ice, and melt ponds. Snow fraction and pond fraction are parameterized in terms of the predicted snow and pond depths, respectively. The bare ice fraction can then be calculated as a residual. In regions covered with sea ice, the surface albedo is a weighted average of the ice albedo (1) and the water albedo of about 7% (depending on solar zenith angle). The albedos used in (1) are based on empirical formulae [cf. *Pedersen et al.*, 2009, Table 2], defined separately for direct/diffuse radiation and for visible/near-infrared bands depending on sea ice thickness, pond depth and snow aging which is parameterized in terms of temperature, snowfall, dirt and soot [*Dickinson et al.*, 1993].

[10] The temporal evolution of melt ponds is calculated from the following prognostic equation

$$\rho_w \frac{\partial \overline{h_p}}{\partial t} = -\rho_i \left(\frac{\partial h_i}{\partial t}\right)_{surfmelt} - \rho_i f_p \left(\frac{\partial h_{pi}}{\partial t}\right)_{melt/freeze} - \rho_w f_p \left(\frac{\partial h_p}{\partial t}\right)_{drain} \quad (2)$$

where $h_p = \overline{h_p}/f_p$ is the pond depth representative for the ponded area, f_p is the pond fractional area, h_i the sea ice thickness in the ice covered part of the grid cell, h_{pi} the thickness of pond ice, and ρ_w, ρ_i are specified densities of water and ice, respectively. The overbar denotes an average over the sea ice covered part of the grid cell. The first term on the r.h.s. of (2) represents the production of meltwater through surface melting of sea ice, $\left(\frac{\partial h_i}{\partial t}\right)_{surfmelt} = -\frac{F_m}{\rho_i L_f}$, where L_f is the latent heat of fusion, and F_m is the melt flux defined by equation (11). Note that F_m includes already the effect of melt ponds through both the pond fraction f_p and surface heat fluxes calculated separately for the ponds. This is described in more detail in section 2.2. The second term refers to the formation, growth or melting of pond ice. A simple pond ice model is used providing surface temperature and ice thickness, thus allowing to determine the closing/opening of the pond. Pond ice is formed when the cooling of the pond is large enough to create a slab of ice of at least 1 mm thickness. The pond is temporally closed for $h_{pi} \geq 1$ cm, whereafter the pond may reopen again depending on the net surface heat flux over the pond ice. The third term on the r.h.s. represents the drainage of meltwater to the ocean which is set at a constant rate following *Lüthje et al.* [2006]. The pond fraction f_p is parameterized as a function of $\overline{h_p}$, separately for multiyear ice (MYI) and first year ice (FYI), using results from a small-scale melt pond model [*Lüthje et al.*, 2006; *Pedersen et al.*, 2009]. Both f_p and h_p modify the ice albedo, the melt flux and the conductive heat flux as discussed in section 2.2. The final closing of the pond in fall is generally caused by vanishing ice melt together with drainage of pond water, resulting in $h_p = 0$, or by fall freeze-up when a thick pond ice layer of at least 10 cm is formed.

[11] The scheme described above involves a number of simplifications:

[12] 1. The flux of rain is ignored in (2). This can be justified because, throughout the melt season, the rain flux is an order of magnitude smaller than F_m/L_f, corresponding to the first term on the r.h.s. of (2).

[13] 2. Melt ponds start to form once the snow on ice is completely melted away so that melting snow cannot contribute to pond evolution according to equation (2). This assumption is less justified because in the beginning of the melt season ponds and snow may actually coexist [e.g., *Perovich et al.*, 2002a].

[14] 3. Meltwater drainage is set at a constant rate, $\left(\frac{\partial h_p}{\partial t}\right)_{drain} = 1.39 \times 10^{-7}$ m/s, corresponding to 1.2 cm/day. This can be interpreted as vertical percolation of meltwater through connected pore structures in the ice assuming constant permeability. However, as shown by *Polashenski et al.* [2012], the permeability is often abruptly changing, resulting in a highly variable loss of meltwater. Horizontal meltwater transport is not taken into account. The drainage rate is used as a tuning parameter in our scheme.

[15] 4. The sea ice model remains unchanged. The melt pond scheme is part of the atmosphere model and the advection of pond water is ignored. The only interaction between the sea ice model and the melt pond scheme is through the reduction of the ice albedo, resulting in an enhanced melt flux passed to the sea ice model.

[16] A crucial element of current melt pond schemes applied in climate models [*Holland et al.*, 2012; *Pedersen et al.*, 2009] is the parameterization of pond fraction in terms of pond depth. *Polashenski et al.* [2012], for example, show that both schemes are able to capture only part of the observed evolution of pond fraction when forced with observed pond depths, and suppose that such a relationship cannot be represented by any function.

2.2. Sea Ice Melt

[17] The surface melt of sea ice is the basic parameter determining the evolution of melt ponds in spring and summer. Once the snow is melted away, the surface temperature of bare ice (subscript b) is calculated from the heat budget of a thin surface layer $h_0 = 10\ cm$ with heat capacity $C_i = \rho_i c_{p,i} h_0$:

$$C_i \frac{\partial T_{i,b}}{\partial t} = H_{sfc,b} + H_{c,b} \tag{3}$$

The conductive heat flux through bare ice is proportional to the vertical temperature gradient:

$$H_{c,b} = \frac{k_i}{h_i}(T_{bot} - T_{i,b}) \tag{4}$$

with

[18] $c_{p,i}$=specific heat of sea ice at constant pressure

[19] k_i= thermal conductivity of sea ice

[20] $T_{i,b}$= surface temperature of bare sea ice

[21] T_{bot}= temperature at the bottom of the ice, fixed at the freezing point of seawater (−1.8°C)

[22] The net surface heat flux on bare ice, $H_{sfc,b}$, is a function of bare ice temperature, bare ice albedo, emissivity, roughness length and atmospheric state variables. The pond temperature and the ice temperature at the base of the pond are always fixed at the melting point, $T_m = 0$°C. Any surplus or deficit of heat caused by the net surface heat flux together with the conductive heat flux through the sea ice below the pond is used for further melting of sea ice or for pond ice formation. The net surface heat flux over melt ponds, $H_{sfc,p}$, is calculated in a way analogous to that over bare ice, except that the ice temperature is replaced by T_m, the bare ice albedo by the pond albedo, and the roughness length for ice replaced by that for water. Once the pond is temporally closed because of ice formation, the depth dependent melt pond albedo is replaced by a specified albedo of 30%, T_m is replaced by the pond ice temperature, and the roughness length for ice is applied.

[23] Melting of sea ice below an open pond depends on the amount of heat available for warming the meltwater above the melting point. In this case, the pond temperature is kept at the melting point, while the net heat flux at the pond surface is used to calculate a "preliminary" ice temperature at pond base, $T^*_{i,p} > T_m$, which is used for melting and thereafter reset to T_m again. An alternative approach would be to initially heat the pond water temperature above T_m, then use the surplus heat content of the pond for melting the ice below the pond, and finally reset the pond temperature to T_m.

[24] The formalism of the melt flux calculation is outlined as follows:

[25] Analogous to (3), the heat budget for the ice below the pond can be written as

$$C_i \frac{\partial T^*_{i,p}}{\partial t} = H_{sfc,p} + H_{c,p} \tag{5}$$

with

$$H_{c,p} = \frac{k_i}{(h_i - h_p)}(T_{bot} - T_m) \tag{6}$$

The discretized versions of (3) and (5) yield "preliminary" temperatures denoted by an asterisk

$$\left[T^{n+1}_{i,b}\right]^* = \frac{\frac{C_i}{\Delta t} T^n_{i,b} + H_{sfc,b} + \frac{k_i}{h^n_i} T_{bot}}{\frac{C_i}{\Delta t} + \frac{k_i}{h^n_i}} \tag{7}$$

and

$$\left[T^{n+1}_{i,p}\right]^* = \frac{\frac{C_i}{\Delta t} T_m + H_{sfc,p} + \frac{k_i}{\left(h^n_i - h^n_p\right)} T_{bot}}{\frac{C_i}{\Delta t} + \frac{k_i}{\left(h^n_i - h^n_p\right)}} \tag{8}$$

where the superscripts n and n_{+1} denote the respective time levels, and Δt is the time step. Once these temperatures are in excess of the melting point T_m, sea ice starts to melt whereafter $\left[T_{i,b}^{n+1}\right]^*$ and/or $\left[T_{i,p}^{n+1}\right]^*$ are reset to T_m. The respective surface melt fluxes are given by

$$F_{m,b} = \frac{C_i}{\Delta t}\left(\left[T_{i,b}^{n+1}\right]^* - T_m\right) + H_{sfc,b} - \frac{k_i}{h_i^n}(T_m - T_{bot}) \quad (9)$$

and

$$F_{m,p} = \frac{C_i}{\Delta t}\left(\left[T_{i,p}^{n+1}\right]^* - T_m\right) + H_{sfc,p} - \frac{k_i}{\left(h_i^n - h_p^n\right)}(T_m - T_{bot}) \quad (10)$$

Finally, the total surface melt flux is defined as a weighted average of the melt flux over bare ice (9) and over melt ponds (10), respectively, with the melt pond fraction f_p as weighting factor:

$$F_m = (1 - f_p)F_{m,b} + f_p F_{m,p} \quad (11)$$

Analogously, the total conductive heat flux through the sea ice is given as

$$H_c = (1 - f_p)H_{c,b} + f_p H_{c,p} \quad (12)$$

Both F_m and H_c are passed to the sea ice model. The meltwater generated through F_m is used in equation (2) for the formation or deepening of melt ponds.

2.3. Model Experiments

[26] Two model configurations were used to isolate the impact of melt ponds on Arctic sea ice. In the standard MPI-ESM-LR, the ponds were accidentally ignored in the calculation of sea ice melt. Thus, the total melt flux (11) and the conductive heat flux (12) included contributions from the bare ice fraction only, resulting in $F_m = F_{m,b}$ and $H_c = H_{c,b}$. Ponds are actually simulated in this model as described in section 2.1, including their effect on the ice albedo according to the definition (1), however, the interaction between pond evolution, ice albedo and ice melt is missing. Thus, ponds can be considered inactive in this model. In the alternative model, the ponds are activated, i.e., the melt flux and the conductive heat flux are defined according to equations (11) and (12), respectively.

[27] To compensate for the expected decrease in sea ice in the pre-industrial active-pond (AP) simulation, the geometrical configuration of sea ice growth (lateral vs. vertical) is modified. As discussed in the beginning of section 2, this ratio is governed by the non-dimensional leadclose parameter, c_{freeze}, which can be varied between 0 and 1. The default value, used in the no-pond (NP) simulations, is 2/3. As shown by *Mauritsen et al.* [2012], a higher value of 0.99 increases the Arctic sea ice volume by about 4.5×10^3 km^3, almost independent of season, corresponding to a change of roughly 20% in the annual mean. There is also a modest increase in Arctic sea ice area of about 0.4×10^6 km^2, corresponding to 4% in the annual mean. In the AP experiment, c_{freeze} is increased more moderately to 0.75 which is sufficient to compensate for the loss of ice volume caused by melt ponds in the pre-industrial control experiment. Using the results of *Mauritsen et al.* [2012] as a reference, and applying linear scaling, the additional sea ice caused by the increase in c_{freeze} alone would amount to about 10^3 km^3 in Arctic sea ice volume, corresponding to 5% in the annual mean, and to about 10^5 km^2 in Arctic sea ice area, corresponding to 1% in the annual mean (both with reference to the NP pre-industrial control simulation).

[28] In addition, upper limits were introduced for the pond fractions, i.e., $f_p(MYI) \leq 0.25$ and $f_p(FYI) \leq 0.5$. These modifications with respect to the reference model are motivated by the attempt to simulate similar ice conditions in both pre-industrial control experiments, allowing to start from similar initial states in the respective historical experiments. Otherwise, different trends in the historical and scenario simulations could possibly be attributed to different baseline sea ice thickness distributions [*Boé et al.*, 2009a; *Holland and Bitz*, 2003]. A direct interference between the effects of melt pond activation and modified lead closing in the AP model seems unlikely because both processes operate in different seasons. Furthermore, the sea ice area appears to be insensitive to the modest increase in c_{freeze} applied in the AP model. This enhances the probability that potential differences (AP-NP) in the response of Arctic sea ice to global warming can primarily be attributed to the effects of melt ponds.

[29] Three types of model experiments were performed with both model versions

[30] 1. Pre-industrial unforced control experiments (CTL_NP and CTL_AP) with prescribed concentrations of greenhouse gases and aerosols as of year 1850.

[31] 2. Historical experiments (1850–2005) with time dependent anthropogenic and natural radiative forcings (HIS_NP and HIS_AP).

[32] 3. The historical experiments were extended until year 2100 by applying the Representative Concentration Pathway RCP45, a scenario where the radiative forcing is stabilized at about 4.5 W/m^2 after year 2100 [*Moss et al.*, 2010]. These experiments are denoted by RCP45_NP and RCP45_AP, respectively.

[33] Three realizations were done for HIS_NP and RCP45_NP, but only one for HIS_AP and RCP45_AP. The CTL_NP, HIS_NP and RCP45_NP simulations are part of the contributions of the Max Planck Institute for Meteorology to the fifth phase of the Coupled Model Intercomparison Project (CMIP5).

3. Results

3.1. Melt Ponds, Sea Ice Albedo, and Sea Ice Melt

[34] As shown in Table 1, the impact of active melt ponds on the pre-industrial global mean climate is very small. Somewhat larger are the differences between

Table 1. Global Annual Mean Climate Variables in 100-Year Pre-industrial Control Experiments

Variable	Units	CTL_NP	CTL_AP
Surface air temperature	°C	13.48	13.51
Total cloud cover	%	63.59	63.53
Column water vapor	kg/m^2	23.08	23.13
Liquid water path	g/m^2	57.86	57.80
Ice water path	g/m^2	31.73	31.44
Total precipitation	mm/d	2.924	2.927
Top-of-atmosphere net shortwave radiation	W/m^2	237.4	237.5
Top-of-atmosphere net longwave radiation	W/m^2	−236.9	−237.0
Top-of-atmosphere net shortwave+longwave radiation	W/m^2	0.521	0.512

CTL_AP and CTL_NP in sea ice area and sea ice volume (Table 2). In the Northern Hemisphere (NH), both ice area and ice volume are slightly smaller in CTL_AP, especially in summer, whereas the opposite is found in the Southern Hemisphere (SH). This differential response can be explained by the asymmetric role of melt ponds which are quite abundant in NH summer but very rare in SH summer in observations [e.g., *Brandt et al.*, 2005], in previous model studies [*Holland et al.*, 2012; *Pedersen et al.*, 2009], and in this study as well (not shown). On the other hand, the change in the geometrical configuration of sea ice growth in CTL_AP (cf. section 2.3) tends to enhance the sea ice volume in both hemispheres, though somewhat less in the Southern Hemisphere [*Mauritsen et al.*, 2012]. The combined effect of melt pond activation and increased leadclose parameter c_{freeze} is a slight decrease of sea ice in the Northern Hemisphere where the additional melting caused by the melt ponds is only partially compensated by an enhanced growth during the winter months. In the Southern Hemisphere, although the ice is less sensitive to a change in c_{freeze} than in the Northern Hemisphere, somewhat more ice is simulated in AP because of the missing compensation through melt ponds. Nevertheless, as discussed in section 2.3, it seems unlikely that the relatively minor differences between the control experiments and the modest tuning of the AP model may exert a dominant influence on the sea ice trends in the historical simulations.

[35] Figure 2 shows the temporal evolution of surface air temperature throughout the transient simulations (HIS and RCP45). At the end of the historical simulations (year 2005), the global mean temperature increased by about 1°C compared to the first 30 years of the historical experiments (1851–1880). In accordance with the imposed RCP45 forcing, the global warming trend in the first half of the 21st century is steeper than in the second half. At the end of the scenario simulation, the global warming amounts to about 2.7°C. The corresponding figures for the Arctic region are around 3°C at the end of the historical period and 6–7°C at the end of the scenario, resulting in a polar amplification factor of 2–3 in both the NP and AP experiments. This is discussed in more detail in section 3.4.

[36] In the following, the focus is on the impact of melt ponds on ice albedo and ice melt in NH summer. It is important to note that pond fraction, ice albedo, and ice melt refer to the ice covered part of the grid box, i.e., these variables are not weighted with the sea ice concentration. Figure 3 shows the geographical distribution of melt ponds and their effect on the ice albedo in the historical simulation HIS_AP during the months with the largest coverage of melt ponds. As expected, there is a clear seasonal cycle in pond fraction. In June, the ponds develop southwards of about 75°N, predominantly in the vicinity of warmer land areas in the Hudson Bay and along the continental shelf. The Atlantic sector, on the other hand, is almost void of ponds because the sea ice boundary is further north and the distance to warmer land areas is rather large. In July, ponds also develop further north, but poleward of about 80°N their coverage remains very small, in contrast to observations where pond fractions $> 10\%$ are generally reported [e.g., *Perovich et al.*, 2009; *Sankelo et al.*, 2010]. Possible reasons for this model failure could be overestimated cloud cover in summer, the simplistic treatment of melt water drainage, and the assumption that melt ponds do not develop unless the snow is completely melted away (cf. section 2.1). In fact, in both the NP and AP simulations the central Arctic is partially covered with melting snow throughout the summer, and remnants of melting snow survive even at the end of the scenario simulations. Further south, ponds are captured

Table 2. Sea Ice Area and Sea Ice Volume in Pre-industrial Control Experiments[a]

	Northern Hemisphere		Southern Hemisphere	
Model Simulation	CTL_NP	CTL_AP	CTL_NP	CTL_AP
Sea ice area (MAR)	14.69	14.45	1.10	1.21
Sea ice area (SEP)	6.03	5.70	12.64	12.95
Sea ice area (ANN)	10.63	10.42	6.10	6.28
Sea ice volume (MAR)	28.86	28.18	0.86	1.00
Sea ice volume (SEP)	12.01	10.78	8.95	9.39
Sea ice volume (ANN)	19.93	18.97	3.36	3.62

[a]Units are 10^6 km^2 for sea ice area and 10^3 km^3 for sea ice volume.

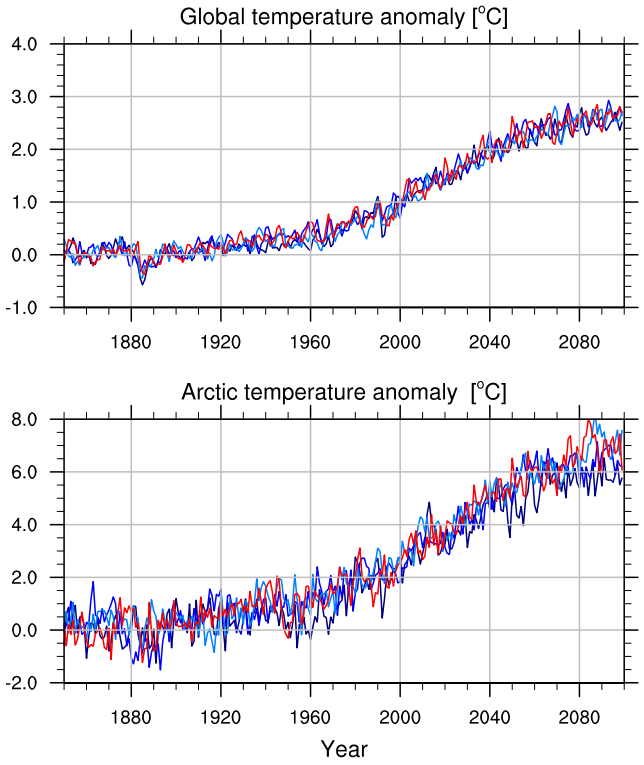

Figure 2. Temporal evolution of annual mean surface air temperature anomalies with respect to the reference period 1851–1880 as simulated in the historical and RCP45 experiments. The Arctic is represented by the area to the north of 70°N. The results from the three NP simulations are shown in blue, those from the AP simulation are shown in red.

more realistically. The largest pond fractions of more than 30% are simulated on FYI along the coasts of Siberia and Alaska and also in the Canadian archipelago. This is in good agreement with observations showing pond fractions on FYI of up to 35% in summer 1998 (http://research.iarc.uaf.edu/belchansky_ccsm/acc2.php). Melt ponds also develop in the East Greenland Sea and in the Barents Sea, but here the pond fractions are comparatively small (< 10%). In August, the ponds start to retreat southwards, and their peak fractions are reduced by more than 10% compared to July. The impact of melt ponds on the ice albedo (Figure 3, right) is a mirror image of the pond concentration, with the ice albedo being reduced by up to 15% in July. The diminished reflection of solar radiation due to $\Delta\alpha_{ice}<0$ can be regarded as an additional radiative forcing compared to the NP simulations in which the higher albedo of unponded ice is applied in the calculation of the surface melt rate. The differences, $\Delta\alpha_{ice}$, shown here are generally much smaller than to be expected from the difference between pond albedo, ranging typically between 25% and 30%, and bare ice albedo, ranging typically between 60% and 65%. The difference of 30%–40% would be realized only if the ice were totally covered with melt ponds.

[37] Figure 4 shows the melt fluxes in the HIS_AP experiment (left panels) and the difference in melt fluxes between HIS_AP and HIS_NP (right panels). In HIS_AP, the ice melt depends on the spatial coverage of melt ponds (cf. section 2.2), whereas in HIS_NP the effect of melt ponds on sea ice melt is ignored. During June and July, the pattern of sea ice melt evolves in close correspondence to the evolution of melt ponds shown in Figure 3 (left). This is expected because, according to equation (2), the ice melt is the main source term in the evolution of melt ponds. Compared to NP, the activation of melt ponds in AP enhances the ice melt (Figure 4, right), consistent with the lowering of the ice albedo.

3.2. Temporal Changes of Melt Ponds, Ice Albedo and Surface Heat Budget

[38] Figure 5 shows the temporal evolution of melt pond patterns (left), their effect on the ice albedo (middle), and the grid-box mean albedo (right) during the month of July in HIS_AP and RCP45_AP, respectively. As the climate warms the summer ice retreats poleward, and the area with largest pond fractions gradually moves northwards from the continental shelf in the present climate to about 75°N during the last 30 years of the scenario simulation. During this period, the central Arctic is covered with melt ponds as well but their fractional coverage is relatively small (generally < 10%). Compared to the last 30 years of the historical simulation, the grid-box mean albedo in the central Arctic decreases by roughly 10% towards the end of the scenario simulation. This is caused by increases in pond coverage and thinning of sea ice but, predominantly, by the diminished sea ice concentration as discussed in section 3.3.

[39] Figure 6 (top) shows a gradual decrease of the ice albedo in response to greenhouse gas forcing. In NP, this decrease is caused by ice thinning, larger pond coverage, and diminished snow cover (not shown). In AP, the positive feedback between increasing pond coverage, decreasing ice albedo, and larger ice melt contributes to a stronger decline in ice albedo. In NP, this feedback is suppressed because ponds are ignored in the calculation of the ice melt (cf. section 2.3). The surface albedo shown in Figure 6 is a weighted average of the ice albedo and the comparatively low water albedo. Consequently, it is substantially smaller than the ice albedo, and the downward trend is more pronounced as well because of the substantial loss of Arctic sea ice in the 20th and 21st centuries, as shown in section 3.3. In AP, the trend in surface albedo is larger than in NP due to the larger trends in both sea ice albedo and sea ice area, indicative of an enhancement of the ice albedo feedback. This is evident also in the absorption of solar radiation in the polar cap northwards of 70°N. In NP, the net surface shortwave radiation increases from 102 W/m^2 in the first 30 years (1851–1880) of the historical simulations to 114 W/m^2 in the last 30 years (2070–2099) of the scenario simulations. This increase is primarily caused by the decrease in surface albedo, though somewhat diminished by changes in the atmosphere such as increasing cloud cover and cloud water content in summer (not shown). The corresponding figures for AP are 103 W/m^2 and 120 W/m^2, respectively.

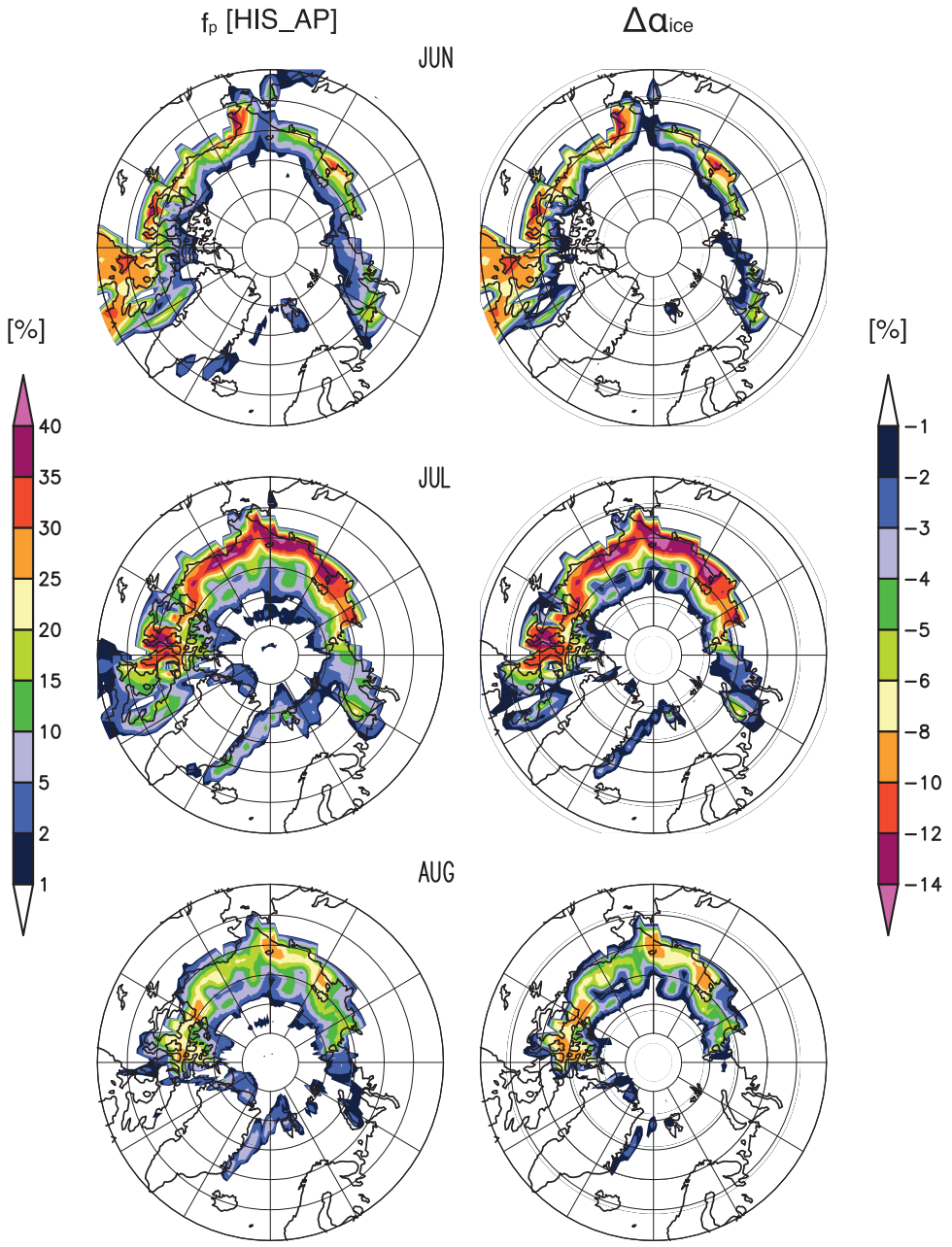

Figure 3. (left) Melt pond fractions in the summer months averaged over the last 30 years (1976–2005) of the historical AP simulation, and (right) difference in sea ice albedo between ponded ice and unponded ice for the same period.

Thus, throughout the 20th and 21st centuries, the absorption of solar radiation at the surface increases by 12 W/m^2 in NP and by 17 W/m^2 in AP.

[40] To identify the primary effect of active melt ponds, the surface heat budget of NH sea ice is shown in Table 3 for both the historical and scenario simulations with and without pond activation in the melt rate term, respectively. In the first 30 years (1851–1880) of the historical simulations, the summer heat budget is dominated by shortwave fluxes of more than 60 W/m^2. Counteracting processes are the net longwave radiation und the turbulent fluxes of sensible and latent heat, respectively. The net flux results in an ice melt of more than 20 cm/month. Due to the smaller ice albedo in AP (cf. Figure 6), the shortwave radiation is enhanced by about 4 W/m^2 compared to NP. The longwave flux, on the other hand, remains virtually unchanged and the turbulent fluxes are just slightly higher than in NP. Consequently, the ice melt in AP is systematically larger than in the NP experiments.

[41] The basal ice growth is proportional to the temperature gradient through the ice. Since the ocean temperature is fixed at the freezing point, the growth during fall and winter is governed by the surface

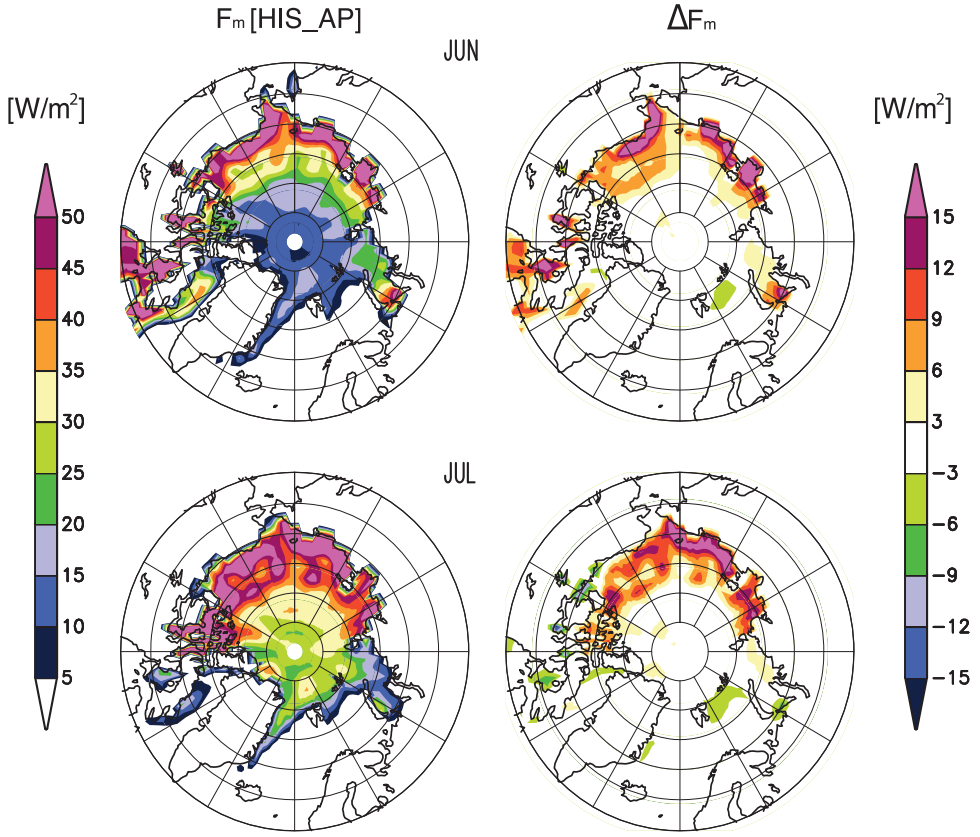

Figure 4. (left) Sea ice melt fluxes in June and July averaged over the last 30 years (1976–2005) of the historical AP simulation, and (right) difference in melt fluxes between AP and NP experiments for the same period.

temperature and the thickness of the ice. During the "pre-industrial" period shown in Table 3, the slightly warmer surface in AP tends to decrease the ice growth compared to NP, whereas the slightly thinner ice tends to increase the growth. Consequently, the difference (AP-NP) in basal growth is relatively small.

[42] In the 20th century, the ice melt increases in all experiments, and all terms in the surface heat budget contribute to this increase. Although the longwave emission from the warmer surface increases, the longwave cooling of the surface is reduced due to enhanced downwelling longwave radiation caused, predominantly, by increased cloudiness in summer (not shown). Moreover, the turbulent heat exchange between the ice and the atmosphere is reduced due to the stabilization of the atmospheric boundary layer: In summer, the surface temperature cannot exceed the melting point unless the ice is completely melted away, whereas the atmosphere is gradually heated in the course of the simulations. The increase in shortwave radiation and also the effect of pond activation on this change are relatively modest and primarily caused by the respective decreases in ice albedo (cf. Figure 6), though somewhat diminished by increasing cloudiness over the polar ice cap. The enhanced basal ice growth in fall and early winter tends to counteract the enhanced summer melt which can be reckoned as a negative feedback [Bitz and Roe, 2004]. The larger basal growth in the 20th century is caused by the NH ice thinning of more than 0.5 m, but diminished by a surface warming of about 2°C.

[43] The changes in the 21st century are qualitatively similar but stronger, and the effect of melt pond activation on the centennial trends in net shortwave radiation and ice melt is more evident than in the 20th century. In NP, as in the 20th century, the increased ice melt is caused mainly by increasing downwelling longwave radiation, followed by reduced sensible heat flux, enhanced absorption of shortwave radiation, and reduced latent heat flux. In AP, on the other hand, as a result of the substantial decrease of ice albedo in the last few decades of the AP simulation (cf. Figure 6), the enhanced absorption of shortwave radiation contributes most to the increase in ice melt. To some extent, these results can be compared to those obtained in global warming simulations by *Holland et al.* [2012]. Although the warming is realized through CO_2 doubling, the global radiative forcing of about 4 W/m^2 is similar to that applied at the end of the RCP45 scenario. In these simulations, the effect of melt ponds on the net shortwave radiation over Arctic sea ice increases from 3 W/m^2 in the control experiment to 6 W/m^2 in the 2xCO_2 experiment. A doubling of the melt pond effect with respect to the first 30 years of the historical simulations can also be inferred from Table 3, though the absolute values are slightly higher (4 and 8 W/m^2, respectively).

[44] The ice thickness in fall and early winter is further decreased by about 1 m. Despite the marked surface

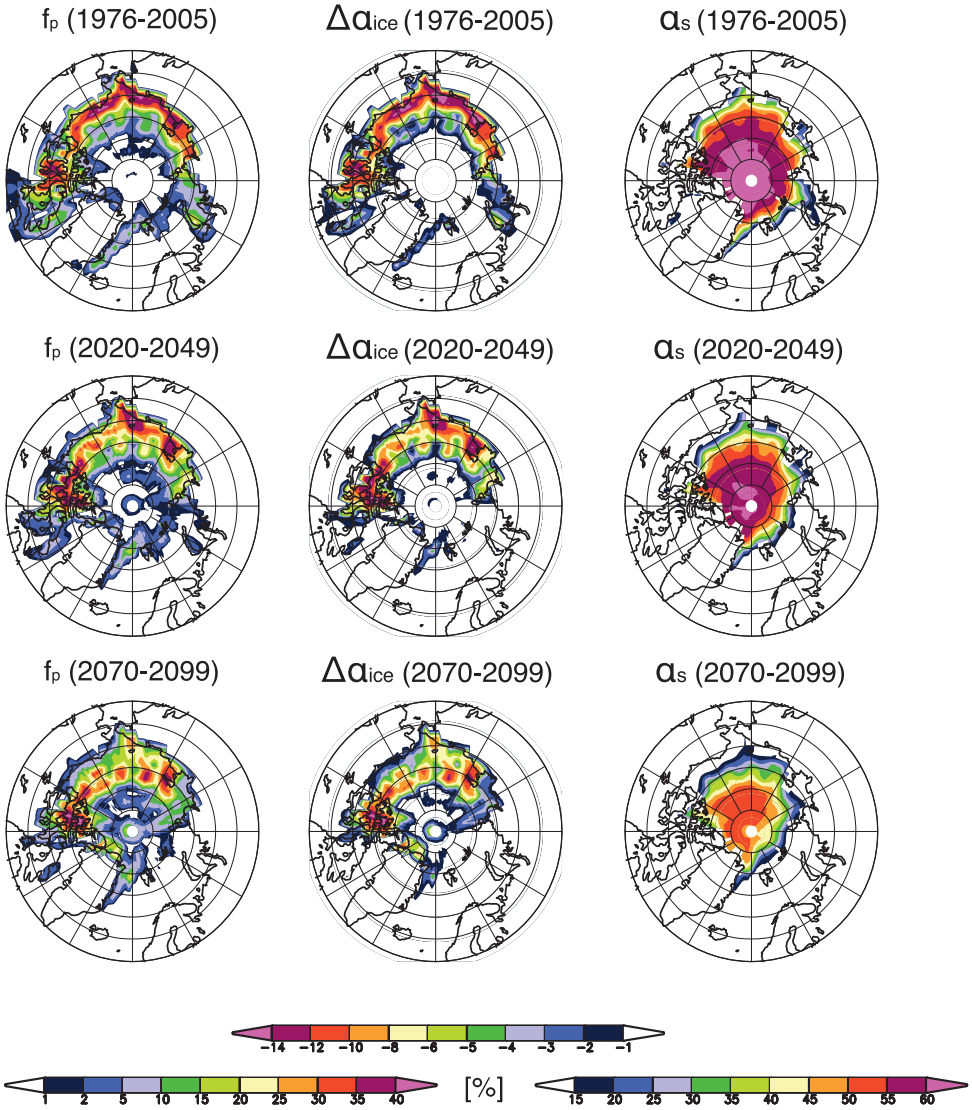

Figure 5. (left) July melt pond fractions in three time slices of the historical and RCP45_AP simulations, (middle) the corresponding differences in sea ice albedo between ponded and unponded ice, and (right) grid-box mean sea ice albedo including open water.

warming, about three times larger than in the 20th century, the change in basal ice growth is larger than before, and continues to counteract the positive trend in ice melt. This effect is more evident in NP than in AP. Due to the larger (smaller) trends in surface ice melt (basal ice growth) in AP, the centennial change of (melt minus growth) is about 2.5 cm/month larger than in NP. The respective difference in the 20th century is just about 0.7 cm/month. Note that these figures refer to the main melting/freezing seasons.

3.3. Sea Ice Cover and Sea Ice Thickness

[45] Figure 7 (left) shows the evolution of September sea ice concentration in the pre-industrial control simulation (CTL_AP), at the end of the historical simulation (HIS_AP) and at the end of the scenario simulation (RCP45_AP). Compared to CTL_AP, the sea ice boundary in HIS_AP is generally further north, and the concentration in the central Arctic is reduced by almost 10%. The shrinking of September ice continues throughout the RCP45_AP simulation so that only a small sea ice area is left during the last 30 years, with concentrations of less than 40% in the central Arctic. The difference of sea ice concentrations between the respective AP and NP simulations is shown at the right hand side of Figure 7. In the CTL and HIS simulations, the differences (AP-NP) are predominantly negative and largest along the continental shelf, from the Laptev Sea eastward to the Canadian archipelago. In the last 30 years of the RCP45 simulations the difference pattern is shifted to the central Arctic. The negative differences (AP-NP) in sea ice concentration are consistent with the respective differences in ice albedo, surface albedo, net shortwave radiation and sea ice melt discussed in section 3.2 (see also Figure 6 and Table 3).

[46] The temporal change in September ice thickness is shown in Figure 8 (left). In the pre-industrial climate, and at the end of the historical period as well, the

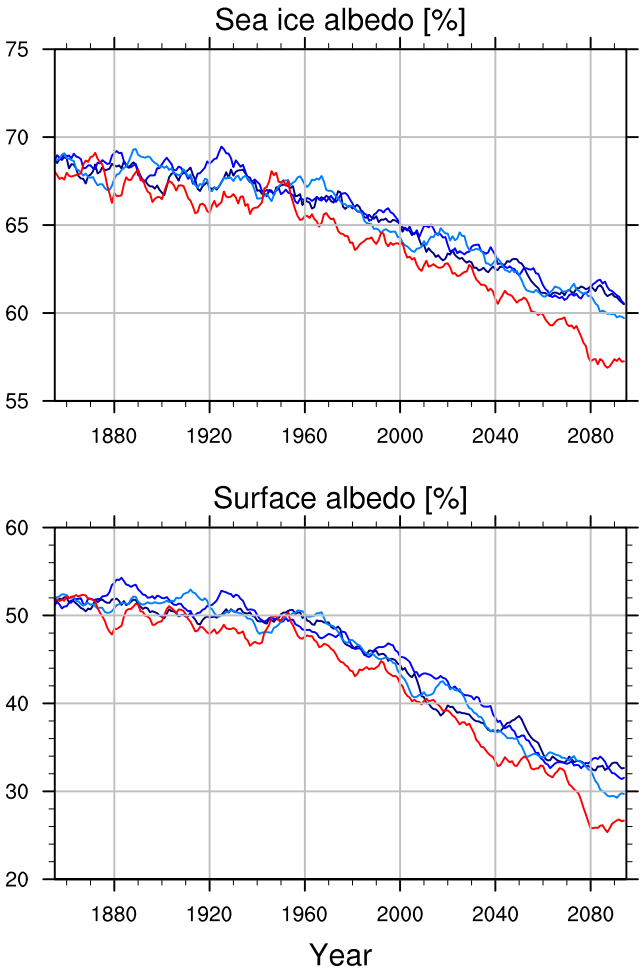

Figure 6. Temporal evolution of July (top) sea ice albedo and (bottom) surface albedo (including open water) in the region northwards of 70°N. The results from the three NP simulations are shown in blue, those from the AP simulation are shown in red, and 11-point running averages are applied for curve smoothing.

thickest ice of more than 3 m and 2 m, respectively, is found north of Greenland. At the end of the scenario simulation, the ice has retreated to the central Arctic Ocean, with a peak ice thickness of about 0.5 m. The difference between experiments AP and NP shows similar patterns as found already for the ice concentration (cf. Figure 7, right). In CTL_AP and HIS_AP, the thinning of the ice is largest along the continental shelf, but even in regions with no or little difference in ice concentration (e.g., north of Greenland and the Canadian archipelago at the end of the historical simulations), the ice in the AP simulations is typically 20–30 cm thinner than in the NP simulations. During the last 30 years of RCP45_AP, the remaining ice in the central Arctic is about 20 cm thinner than in RCP45_NP. The spatially coherent differences (AP-NP) in sea ice thickness throughout the 20th and 21st centuries are primarily caused by the systematic reduction in ice albedo (cf. Figure 6) in response to the activation of melt ponds. This decrease in ice thickness contributes to the respective change in ice concentration, because in order to achieve the same loss of ice covered area, a smaller volume of ice must be melted. Additionally, thinner ice is more susceptible to surface melting because the ice albedo decreases with decreasing ice thickness.

[47] Owing primarily to the seasonality of melt pond coverage but also to the larger susceptibility of thinner ice to a radiative forcing, the differences between the AP and NP experiments are most pronounced in summer and fall (July through November). This is evident from Figure 9 which compares the seasonal cycle of NH sea ice area in the CTL, HIS and RCP45 experiments, respectively. In general, the three members of the NP ensemble are close together, except for one RCP45_NP member at the end of the simulation lying midway between the two other NP members and the AP simulation. In all experiments (CTL, HIS, RCP45), the sea ice area in AP is lower than in all NP simulations. In addition, the differences (AP-NP) gradually increase in the course of the simulations which could be an indication for a modest impact of melt ponds on sea ice trends. At the end of the historical simulations, 1979–2005, both model versions are able to reasonably capture both the amplitude and phase of the observed seasonal cycle. From December to June, the differences (AP-NP) and also the differences between simulations and observations are small, whereas the melt phase from July to September is better captured in AP. Thus, melt ponds tend to increase the amplitude of the seasonal cycle and contribute to a better agreement with the observed one. However, both model versions underestimate the fall freeze-up from September to October.

3.4. Sea Ice Trends and Sensitivities

[48] The temporal evolution of NH sea ice extent in September is shown in Figure 10. All experiments are characterized by marked natural variability at interannual and longer time scales. Most evident are the abrupt reductions in sea ice extent within less than a decade followed by a fast recovery. In the historical AP simulation, for example, the sea ice extent dropped from 7.2×10^6 km^2 in year 1996 to 4.3×10^6 km^2 in 2005, as observed in year 2007. However, unlike the observed sea ice, it recovered to almost 6×10^6 km^2 within the following 4 years. Even more extreme is the decrease of 3.6×10^6 km^2 within one year in the RCP45_AP simulation, from 4.5×10^6 km^2 in year 2049 to 0.9×10^6 km^2 in 2050, followed by an increase to about 4.0×10^6 km^2 within 5 years. A similar behavior is found in other models as well, and probably caused by anomalous poleward heat transport [*Holland et al.*, 2006; *Graversen et al.*, 2011]. As shown in Figure 11, the strong variability in sea ice extent is also reflected in the respective 26-year overlapping trends simulated in the historical simulations. A length of 26 years was chosen because this is the longest one in the historical simulations for which satellite data were available (1979–2005). Due to the large internal variability of the Arctic climate system simulated on this time scale, the impact of melt ponds on the surface heat budget in

Table 3. Heat Budget Terms and State Variables of the Northern Hemisphere Sea Ice in the NP and AP Experiments[a]

Variables	Months	NP_1	NP_2	NP_3	NP_ens	AP
1851–1880						
Net shortwave radiation (W/m^2)	JJA	61.4	61.2	61.7	61.4	65.7
Net longwave radiation (W/m^2)	JJA	−19.2	−19.4	−19.5	−19.4	−19.5
Sensible heat flux (W/m^2)	JJA	−3.86	−3.81	−3.41	−3.69	−4.24
Latent heat flux (W/m^2)	JJA	−8.76	−8.75	−8.59	−8.70	−9.14
Surface ice melt (cm/month)	JJA	24.3	24.1	24.8	24.4	27.5
Basal ice growth (cm/month)	OND	16.3	15.8	16.3	16.1	16.5
Sea ice temperature (°C)	OND	−21.3	−21.2	−21.3	−21.3	−20.8
Sea ice thickness (m)	OND	2.03	2.17	1.95	2.05	1.98
(1976–2005) – (1851–1880)						
Net shortwave radiation (W/m^2)	JJA	0.54	0.85	0.67	0.69	1.64
Net longwave radiation (W/m^2)	JJA	2.15	2.00	2.30	2.15	2.05
Sensible heat flux (W/m^2)	JJA	1.05	0.96	0.47	0.83	1.16
Latent heat flux (W/m^2)	JJA	0.63	0.58	0.39	0.53	0.75
Surface ice melt (cm/month)	JJA	3.21	3.27	2.74	3.07	4.25
Basal ice growth (cm/month)	OND	0.90	1.58	1.61	1.36	1.85
Sea ice temperature (°C)	OND	2.21	1.77	2.27	2.08	2.32
Sea ice thickness (m)	OND	−0.58	−0.70	−0.60	−0.63	−0.72
(2070–2099) – (1976–2005)						
Net shortwave radiation (W/m^2)	JJA	1.73	2.00	2.12	1.95	4.70
Net longwave radiation (W/m^2)	JJA	3.28	3.75	3.85	3.63	3.70
Sensible heat flux (W/m^2)	JJA	1.09	0.98	1.11	1.06	0.97
Latent heat flux (W/m^2)	JJA	0.95	0.94	1.03	0.97	0.91
Surface ice melt (cm/month)	JJA	4.79	5.15	5.55	5.16	7.32
Basal ice growth (cm/month)	OND	2.60	2.34	2.56	2.50	2.18
Sea ice temperature (°C)	OND	5.87	6.36	7.03	6.42	7.67
Sea ice thickness (m)	OND	−0.99	−1.03	−0.98	−1.00	−0.95

[a]Shown are results for a ''pre-industrial'' period and the respective changes in the 20th and 21st centuries. Heat fluxes contributing to surface cooling are indicated by a negative sign. NP_ens denotes the ensemble mean.

the historical simulations (cf. Table 3) is insufficient to produce a noticeable increase in the trends of sea ice extent, and only very few simulated trends can be found in the two standard deviation range of the observed data. Notable is the wide range of simulated trends between 1950 and 2005. This is even more evident in the overlapping 26-year trends shown in Figure 12 characterized by marked multidecadal variability in both the historical and scenario simulations. However, this apparent variability in the overlapping trends should not necessarily be attributed to multidecadal variability of the Arctic climate system but could also be triggered by sea ice variability at much shorter time scales. In all four experiments periods with strong negative trends of -0.8×10^6 to -1.0×10^6 km^2/decade are followed by periods with weak or even positive trends. In 1979–2011, the observed 26-year downward trends are systematically larger than the simulated ones. Incidentally, the trend evolution in one simulation resembles the observed one, except for a time shift of about 5 years. If the natural variability evident in all simulations is a realistic feature, an attenuation of the Arctic sea ice decline could be expected within the forthcoming decades.

[49] In Table 4, linear trends in September NH sea ice extent are summarized for both the historical and scenario simulations. During the first 100 years of the historical simulations, the trends are already downward but small, i.e., around −0.6%/decade in the NP experiments and slightly larger (−1.0%/decade) in the AP experiment. Due to the accelerated warming in the last 50 years of the historical simulations (cf. Figure 2), the trends are becoming larger but remain clearly below the observed trends in all experiments, the only exception being the extreme decadal trend, 1995–2005, in the HIS_AP simulation which, however, seems to be one of the statistically rare events (cf. Figure 10). The strong variability from interannual to multidecadal time scales noticeable in Figures 10–12, also discussed by *Kay et al.* [2011], is reflected in the simulated trends over the period 1979–2005 varying between −6.53%/decade in the first NP member and +2.55%/decade in the second one. As expected, less variability is found for longer time scales. Within the NP ensemble, the trends calculated for the whole 21st century are rather similar, and they are also systematically larger than in the 20th century, especially the percentage changes. Except for the first 100 years of the historical experiments, the trends in the AP experiments do not stand out. The absolute changes are mostly within the ranges simulated in the NP experiments. However, the percentage changes are generally larger than in NP due to the stronger initial ice reduction in the AP experiment. The sea ice extent left over in September 2100, based on linear trends 2005 to 2100, is smaller than in all NP experiments, and the sea ice vanishes between 8 and 23 years earlier. As discussed in section 3.2 (see also Figure 6 and Table 3), the stronger sea ice decline in AP is consistent with an enhancement of the ice albedo feedback through pond activation.

[50] One of the most robust features of simulated climate change is the polar amplification of anthro-

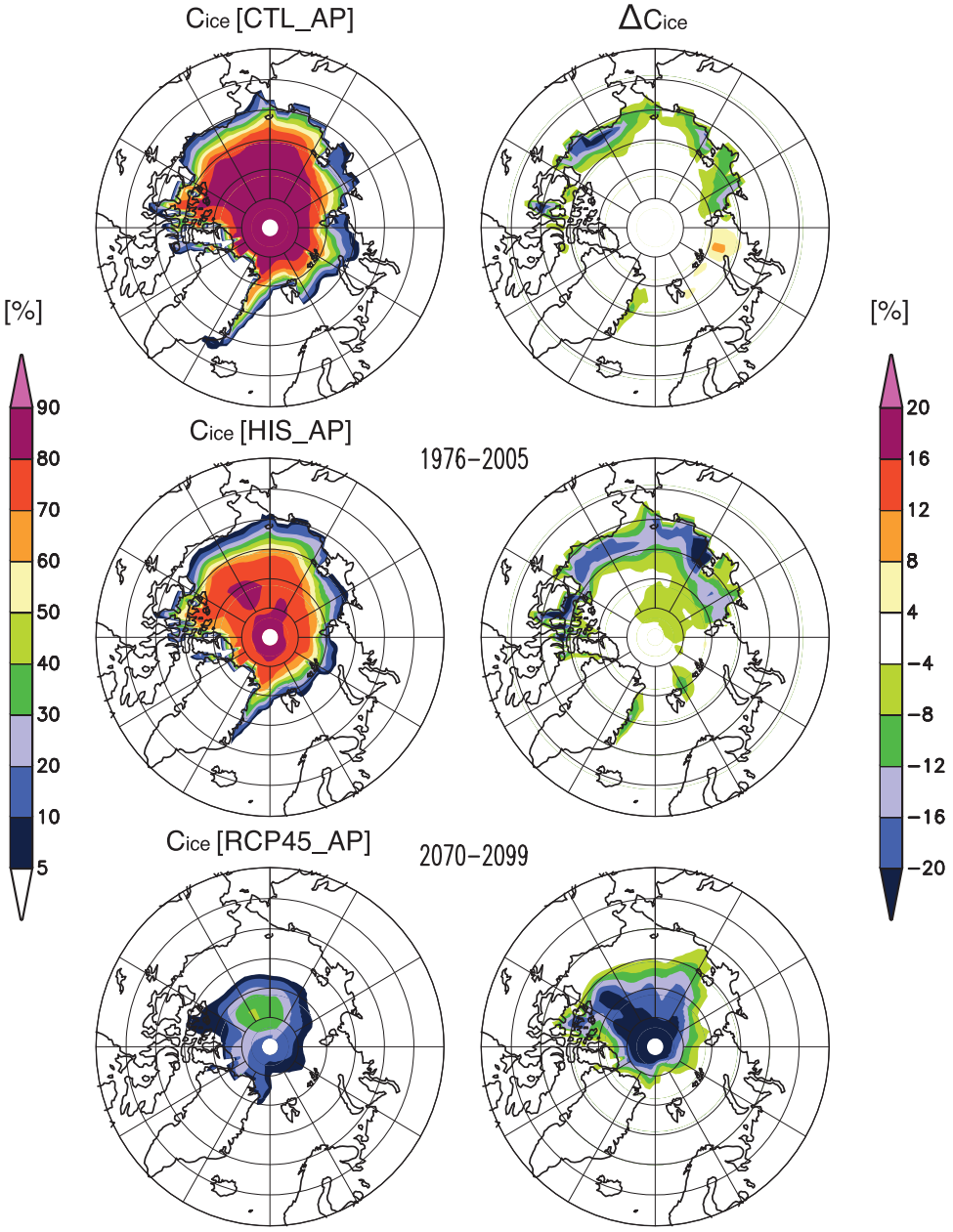

Figure 7. (left) September sea ice concentrations in CTL_AP (100 years), in HIS_AP and in RCP45_AP, and (right) the differences between the corresponding AP and NP experiments.

pogenic temperature change [*Holland and Bitz*, 2003; *Meehl et al.*, 2007]. Figure 13a shows a scatterplot of Arctic vs. global surface air temperature for all of the simulations used in this study. This includes the pre-industrial control runs, indicated by the cloud of points in the low-temperature regime, the historical experiments, and also the RCP45 scenario simulations. Regression lines are plotted separately for the historical and scenario simulations. Around year 2100, the Arctic mean temperature in the AP simulation is between 0.5°C and 1°C higher than in the NP simulations. The amplification factors shown in Table 5 (left column) are in the range of 2.2 to 2.6 which is marginally higher than the multi-model mean of 2.2 simulated in the IPCC AR4 models [*Meehl et al.*, 2007]. Clearly, the polar amplification is almost independent of the amount of radiative forcing. Melt ponds tend to enhance the polar amplification in the RCP45 scenario, but the effect is relatively small. The sensitivity of the Arctic sea ice to global warming can be inferred from Figure 13b which shows a scatterplot of NH sea ice extent vs. global annual mean surface air temperature. The slopes of the regression lines are summarized in Table 5 showing a general amplification of the sensitivity in the RCP45 runs compared to the historical ones. This is particularly evident in September where the sensitivities are increased by more than 50%. The sensitivities obtained for the annual mean ice extent are within the range

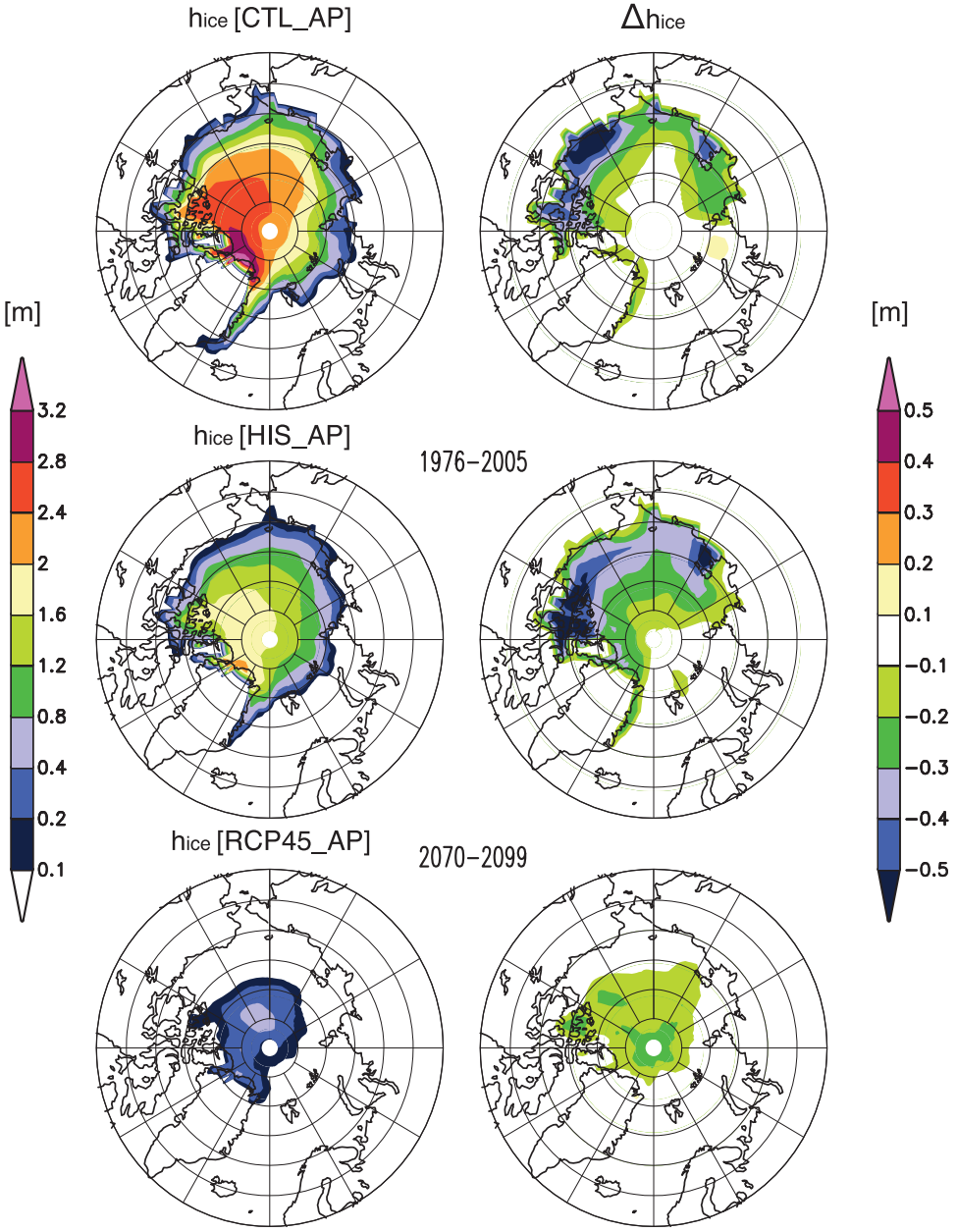

Figure 8. As Figure 7, but for sea ice thickness.

found by *Winton* [2011, Table 3] for a subset of IPCC AR4 models (-0.8 to -1.9×10^6 km^2/K) and are only marginally higher than in the ECHAM5/MPI-OM model (-1.3×10^6 km^2/K). All of these sensitivities are considerably smaller than estimated from observational records of sea ice extent and temperature, 1979–2010, of about -3×10^6 km^2/K. However, as discussed by *Winton* [2011], this apparent sensitivity calculated for a relatively short period is certainly influenced by natural variability (see also Figure 11) and, thus, may not be a sufficiently accurate estimate of the true sensitivity of the climate system. As a result of the enhanced ice albedo feedback in AP, the annual sensitivities are higher than in all of the NP simulations. The difference (AP-NP) is more pronounced in the RCP45 runs (between +7% and +25%) than in the historical ones (between +2% and +11%)

4. Summary and Conclusions

[51] The additional radiative forcing caused by the lowering of the ice albedo in the AP (active pond) simulations leads to a systematic reduction of both sea ice area and thickness through a positive feedback loop resembling the ice albedo feedback in global warming simulations: open ponds → diminished ice albedo → enhanced absorption of solar radiation → enhanced melt flux → increased pond coverage and less sea ice.

[52] At the end of our historical AP simulations, 1976–2005, melt ponds develop predominantly in the

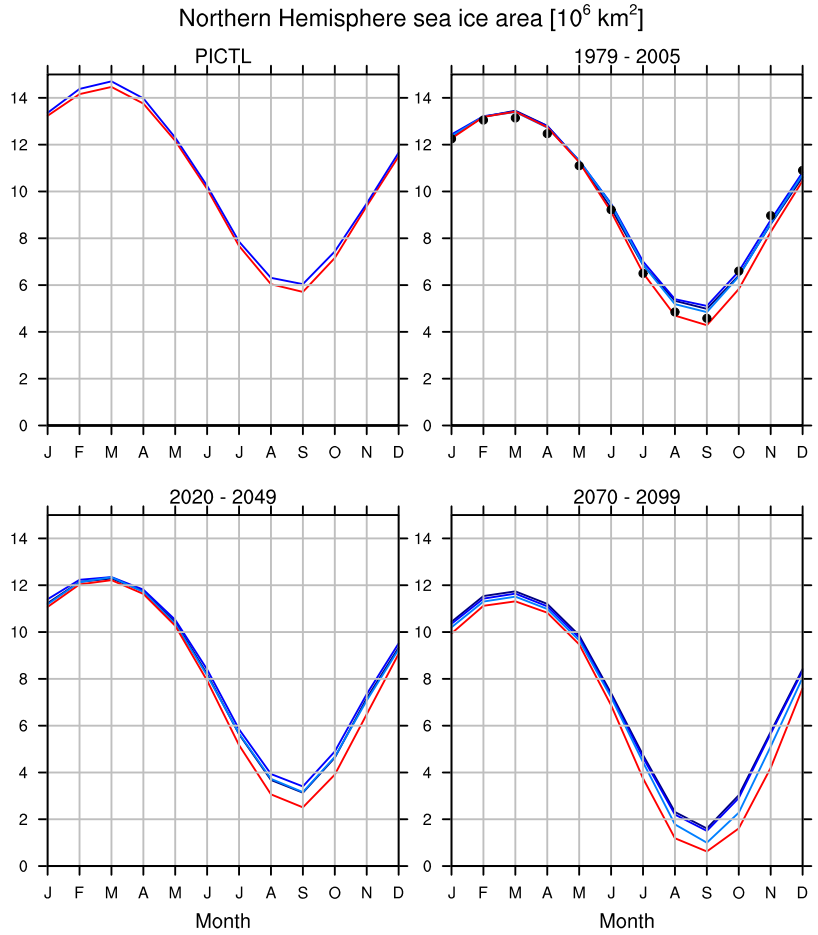

Figure 9. Seasonal cycle of NH sea ice area in the pre-industrial control experiments (PICTL), in the historical simulations averaged over the last 27 years (1979–2005), and in two 30-year time slices of the RCP45 simulations. The results from the NP simulations are shown in blue, those from the AP simulations in red. The climatological seasonal cycle based on the National Snow and Ice Data Center (NSIDC) dataset (1979–2005) is indicated by black dots.

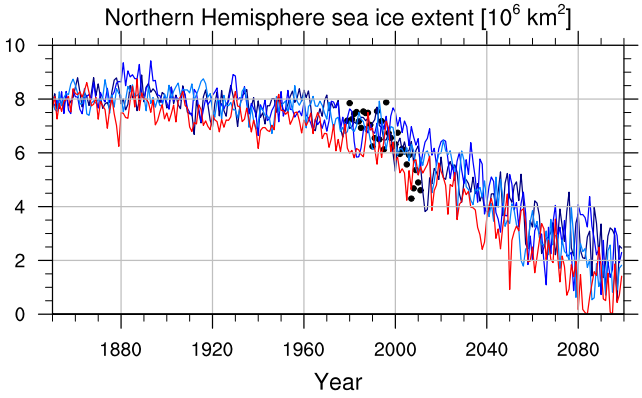

Figure 10. Temporal evolution of September NH sea ice extent as simulated in the historical and RCP45 scenario experiments. The results from the three NP simulations are shown in blue, those from the AP simulation are shown in red. Observations based on the National Snow and Ice Data Center (NSIDC) dataset (1979–2011) are shown as black dots.

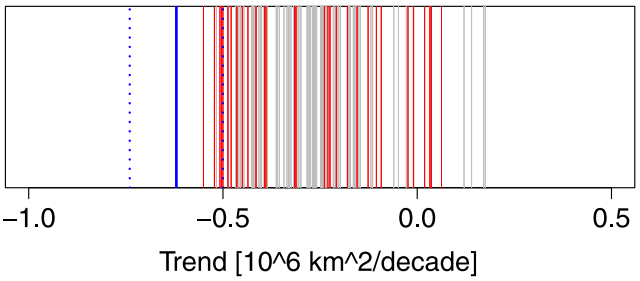

Figure 11. Linear trends in September NH sea ice extent based on 26-year overlapping trend calculations (1950–1976, 1951–1977, ..., 1979–2005). Shown are results from the three historical NP simulations (gray lines) and from the historical AP simulation (red lines). The blue line shows the observed trend (1979–2005) based on the National Snow and Ice Data Center (NSIDC) dataset. The area between the blue dotted lines represents the $\pm$ two standard deviation range of the observed data.

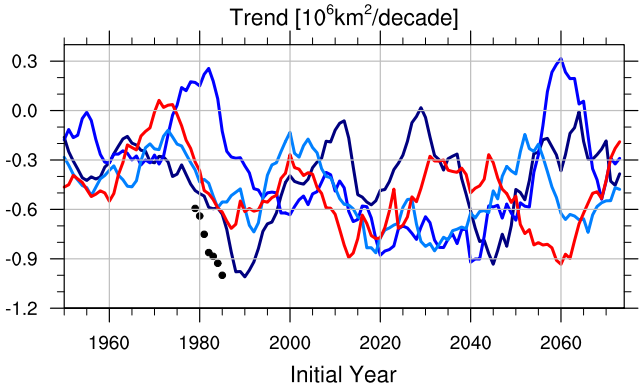

Figure 12. Temporal evolution of overlapping 26-year linear trends in September NH sea ice extent (1950–1976, 1951–1977, ..., 2073–2099) in the historical and RCP45 simulations. The symbols denote observed 26-year trends (1979–2005, 1980–2006, ..., 1985–2011) based on the National Snow and Ice Data Center (NSIDC) dataset.

continental shelf regions along the coasts of Siberia and Alaska and in the Canadian archipelago. As a result, the ice albedo in these regions is systematically smaller than in the NP (no pond) simulations, the melt fluxes are enhanced, and both the ice concentration and ice thickness during the seasonal minimum in September are smaller. On the other hand, the pond coverage in the East Greenland Sea and in the Barents Sea is much smaller, and hardly any ponds are simulated in the central Arctic. Consequently, in these regions, the differences (AP-NP) in ice concentration and ice thickness are very small as well. Although a pond climatology does not yet exist, several in situ observations suggest a widespread pond coverage in the central Arctic [e.g., *Perovich et al.*, 2009; *Sankelo et al.*, 2010]. Possible reasons for the model failure could be, for example, overestimated cloud cover in summer, the simplistic treatment of pond water drainage, or the disputable assumption that melt ponds do not form unless the sea ice is void of snow (cf. section 2.1). The lack of ponds is reflected also in the simulated surface albedo of 55–65% in the central Arctic which is typically 5% higher than that derived from satellite data [*Laine*, 2004].

[53] As the climate warms in the RCP45 scenario, the peripheral seas are gradually becoming ice free in both the AP and NP experiments. In the central Arctic, however, the impact of melt ponds is still evident. Consistent with larger melt fluxes and smaller surface albedo in AP during the last 30 years (2070–2099) of the scenario simulations, both the ice concentration and ice thickness are substantially smaller than in NP. The difference (AP-NP) in NH sea ice area reveals a pronounced seasonality in both the historical and scenario simulations, with maximum values during summer and fall caused primarily by the evolution of melt ponds in late spring and summer but also by the larger susceptibility of thinner ice to radiative forcings. Thus, melt ponds tend to increase the amplitude of the seasonal cycle and contribute to a better agreement with the observed one.

[54] In response to the external forcing prescribed in the historical and scenario simulations, the surface heat budget over ice is gradually increasing in summer. This is not only caused by decreasing ice albedo but, predominantly, by changes in atmospheric state variables resulting in enhanced downwelling longwave radiation and reduced turbulent heat fluxes, i.e., in less surface cooling. The influence of melt pond activation on the trends in the surface heat budget is evident in the increased shortwave radiation and ice melt compared to NP. This is more pronounced in the 21st century where, in contrast to the NP simulations, the shortwave absorption contributes more than the other terms to the centennial increase in surface ice melt. The gradual thinning of the Arctic sea ice also increases the basal ice growth, being inversely proportional to the ice thickness. Towards the end of the scenario simulation this negative feedback, active in fall and winter, is somewhat smaller in AP than in the three NP realizations because of a stronger surface heating.

[55] From the beginning of the historical simulations until the end of the scenario simulations, the solar energy absorbed in summer at the surface of the polar cap northwards of 70°N is increasing by about 12 W/m^2 in NP and 17 W/m^2 in AP. These changes are primarily

Table 4. Linear Trends in September NH Sea Ice Extent[a]

Years	NP_1	NP_2	NP_3	NP_ens	AP	Obs
1850–1953	−0.049 (−0.60)	−0.044 (−0.52)	−0.054 (−0.65)	−0.049 (−0.60)	**−0.080 (−1.00)**	
1953–1979	−0.355 (−4.35)	−0.150 (−1.98)	**−0.421** (−5.21)	−0.309 (−3.89)	−0.415 **(−5.57)**	
1979–2005	**−0.486 (−6.53)**	+0.171 (+2.55)	−0.360 (−5.01)	−0.225 (−3.16)	−0.312 (−4.80)	(−9.12 ± 1.54)
1953–2005	**−0.362** (−4.42)	−0.123 (−1.65)	−0.341 (−4.25)	−0.275 (−3.49)	−0.328 **(−4.45)**	(−7.77 ± 0.60)
1995–2005	−0.394 (−6.07)	−0.028 (−0.40)	−0.631 (−9.44)	−0.351 (−5.18)	**−2.317 (−32.9)**	(−17.91 ± 5.98)
2005–2100	−0.540 (−9.15)	−0.523 (−8.05)	**−0.551** (−8.93)	−0.538 (−8.69)	−0.545 **(−9.90)**	
2100	0.824 (14.0)	1.579 (24.3)	0.995 (16.1)	1.133 (18.3)	0.381 (6.9)	
Year (SIE < 10^6 km^2)	2097	2112	2100	2103	2089	

[a]Results are shown for all historical and future NP and AP experiments. NP_ens denotes the ensemble mean. Units are 10^6 km^2/decade. The respective percentage changes are shown in parentheses. Obs: *Stroeve et al.* [2007] with trends calculated over 1-year longer periods (1979–2006 and 1953–2006, respectively). Second row from below: sea ice extents (10^6 km^2) for year 2100, estimated from linear trends, 2005–2100. Percentage values of year 2005 ice extents are shown in parentheses. Lowest row: Year of "vanishing" sea ice in September (i.e., sea ice extent SIE $< 1.0 \times 10^6$ km^2) estimated from linear trends, 2005–2100. Largest downward trends are highlighted in bold.

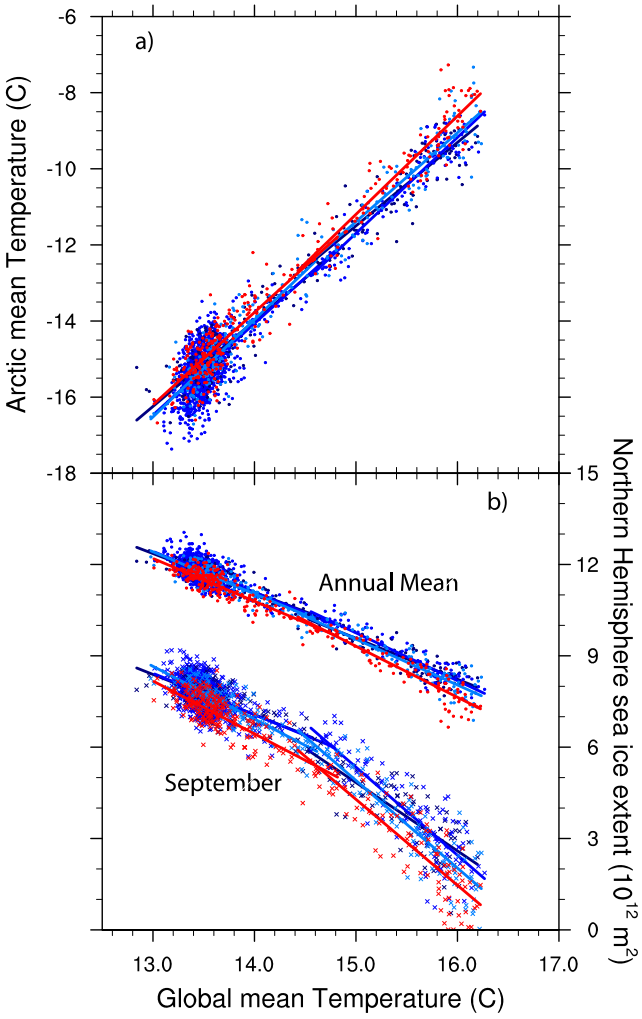

Figure 13. (a) Annual mean Arctic (70°N–90°N) vs. global surface air temperature in the control experiments, in the historical simulations, and in the RCP45 scenario. The NP results are shown in blue, the AP results in red. (b) NH sea ice extent vs. global surface air temperature.

due to decreases in sea ice area and sea ice albedo, both being somewhat more pronounced in AP than in NP, indicative of an enhancement of the ice albedo feedback by means of pond activation. In all simulations but one, the September sea ice in the Northern Hemisphere is projected to vanish at the end of the 21st century. In AP, consistent with a stronger decline of surface albedo compared to NP, this happens between 8 and 23 years earlier than in the three NP realizations. Also, as a result of the enhanced ice albedo feedback in AP, the sensitivity of Arctic sea ice to global warming is higher than in all of the NP simulations.

[56] Over the period of modern satellite observations, 1979–2005, the simulated trends are systematically smaller than those derived from satellite data. This applies to all individual NP realizations and to the AP simulation as well. Obviously, in this rather short period, the effect of melt pond activation is insufficient to substantially enhance the decline of Arctic sea ice and the sensitivity of the Arctic sea ice extent to global warming. This could be possibly related to the inability of the model to produce a significant amount of melt ponds in the central Arctic. The underestimation of sea ice trends since the beginning of the satellite era in 1979 is a common deficiency of current climate models [*Stroeve et al.*, 2007]. More recently, *Winton* [2011] found that none of the models under investigation "has both a temperature trend as small as observed and an ice decline as large" and concluded that all models underestimated the sensitivity of the NH sea ice cover to global warming. In most of these models the treatment of sea ice processes is still rather crude. For example, as in our model, the sea ice is often represented by a single layer only, and a parameterization of a subgrid-scale ice thickness distribution is generally missing. Nevertheless, *Winton* [2011] could not rule out a significant contribution of natural variability to the observed "apparent" sensitivity so that, on this rather short time scale, the difference between models and observations should not necessarily be attributed to inadequate or missing physics. This alternative view is also supported by our model simulations revealing a distinct modulation of the externally driven downward sea ice trends by natural variability.

Table 5. Polar Amplification Factor and Sea Ice Sensitivity in Historical and Scenario Simulations as Derived From the Slopes of the Regression Lines in Figure 13b[a]

Experiment	$\Delta T_A/\Delta T_G$	$\Delta SIE(ANN)/\Delta T_G$ (10^6 km^2/K)	$\Delta SIE(SEP)/\Delta T_G$ (10^6 km^2/K)
HIS_NP_1	2.25	−1.27 (0.90)	−1.32 (0.76)
HIS_NP_2	2.41	−1.34 (0.95)	−1.36 (0.78)
HIS_NP_3	2.55	−1.38 (0.98)	−1.73 (0.99)
HIS_AP	2.43	−1.41	−1.74
RCP45_NP_1	2.19	−1.34 (0.80)	−2.25 (0.80)
RCP45_NP_2	2.52	−1.57 (0.93)	−2.89 (1.02)
RCP45_NP_3	2.34	−1.50 (0.89)	−2.88 (1.02)
RCP45_AP	2.58	−1.68	−2.82

[a]ΔT_G is the change in global and annual mean surface air temperature, ΔT_A is the annual mean temperature change in the Arctic poleward of 70°N, and ΔSIE is the change in Northern Hemisphere sea ice extent. The ratio of the NP sensitivities to the respective AP sensitivities is shown in parentheses.

[57] **Acknowledgments.** We thank Dirk Notz for providing Figure 1 and for his valuable comments on an earlier version of this paper. Special thanks also to two anonymous reviewers for constructive comments that contributed substantially to an improvement of our paper. The model simulations were performed on the IBM power6 supercomputer installed at the German Climate Computing Centre (DKRZ) in Hamburg.

References

Belchansky, G. I., D. C. Douglas, V. A. Eremeev, and N. G. Platonov (2005), Variations in the Arctic's multiyear ice cover: A neural network analysis of SMMR-SSM/I data, 1979–2004, *Geophys. Res. Lett.*, *32*, L09605, doi:10.1029/2005GL022395.

Bitz, C. M., and G. H. Roe (2004), A mechanism for the high rate of sea ice thinning in the Arctic Ocean, *J. Clim.*, *17*, 3623–3632, doi:10.1175/1520-0442(2004)017<3623:AMFTHR>2.0.CO;2.

Boé, J., A. Hall, and X. Qu (2009a), September sea-ice cover in the Arctic Ocean projected to vanish by 2100, *Nat. Geosci.*, *2*, 341–343, doi:10.1038/ngeo467.

Boé, J., A. Hall, and X. Qu (2009b), Current GCM's unrealistic negative feedback in the Arctic, *J. Clim.*, *22*, 4682–4695, doi:10.1175/2009JCLI2885.1.

Brandt, R. E., S. G. Warren, A. P. Worby, and T. C. Grenfell (2005), Surface albedo of the Antarctic sea ice zone, *J. Clim.*, *18*, 3606–3622, doi:10.1175/JCLI3489.1.

Dickinson, R. E., A. Henderson-Sellers, and P. J. Kennedy (1993), Biosphere Atmosphere Transfer Scheme (BATS) version 1e as coupled to the NCAR Community Climate Model, *NCAR Tech. Note, NCAR/TN-387+STR*, 72 pp., Natl. Cent. for Atmos. Res, Boulder, Colo.

Fetterer, F., and U. Untersteiner (1998), Observations of melt ponds on Arctic sea ice, *J. Geophys. Res.*, *103*, 24,821–24,835, doi:10.1029/98JC02034.

Flanner, M. G., K. M. Shell, M. Barlage, D. K. Perovich, and M. A. Tschudi (2011), Radiative forcing and albedo feedback from the Northern Hemisphere cryosphere between 1979 and 2008, *Nat. Geosci.*, *4*, 151–155, doi:10.1038/ngeo1062.

Graversen, R. G., T. Mauritsen, S. Drijfhout, M. Tjernström, and S. Martensson (2011), Warm winds from the Pacific caused extensive Arctic sea-ice melt in summer 2007, *Clim. Dyn.*, *36*, 2103–2112, doi:10.1007/s00382-010-0809-z.

Hibler, W. D. (1979), A dynamic thermodynamic sea ice model, *J. Phys. Oceanogr.*, *9*, 815–846, doi:10.1175/1520-0485(1979)009<0815:ADTSIM>2.0.CO;2.

Holland, M. M., and C. M. Bitz (2003), Polar amplification of climate change in coupled models, *Clim. Dyn.*, *21*, 221–232, doi:10.1007/s00382-003-0332-6.

Holland, M. M., C. M. Bitz, and B. Tremblay (2006), Future abrupt reductions in the summer Arctic sea ice, *Geophys. Res. Lett.*, *33*, L23503, doi:10.1029/2006GL028024.

Holland, M. M., D. A. Bailey, B. P. Briegleb, B. Light, and E. Hunke (2012), Improved sea ice shortwave radiation physics in CCSM4: The impact of melt ponds and aerosols on Arctic sea ice, *J. Clim.*, *25*, 1413–1430, doi:10.1175/JCLI-D-11-00078.1.

Jungclaus, J. H., N. Keenlyside, M. Botzet, H. Haak, J.-J. Luo, M. Latif, J. Marotzke, U. Mikolajewicz, and E. Roeckner (2006), Ocean circulation and tropical variability in the coupled model ECHAM5/MPI-OM, *J. Clim.*, *19*, 3952–3972, doi:10.1175/JCLI3827.1.

Kay, J. E., M. M. Holland, and A. Jahn (2011), Inter-annual to multi-decadal Arctic sea ice extent trends, *Geophys. Res. Lett.*, *38*, L15708, doi:10.1029/2011GL048008.

Laine, V. (2004), Arctic sea ice regional albedo variability and trends, 1982–1998, *J. Geophys. Res.*, *109*, C06027, doi:10.1029/2003JC001818.

Lüthje, M., D. L. Feltham, P. D. Taylor, and M. G. Worster (2006), Modeling the summertime evolution of sea-ice melt ponds, *J. Geophys. Res.*, *111*, C02001, doi:10.1029/2004JC002818.

Marsland, S. J., H. Haak, J. H. Jungclaus, M. Latif, and F. Röske (2003), The Max-Planck-Institute global ocean/sea ice model with orthogonal curvilinear coordinates, *Ocean Modell.*, *5*, 91–127, doi:10.1016/S1463-5003(02)00015-X.

Maslanik, J. A., C. Fowler, J. Stroeve, S. Drobot, J. Zwally, D. Yi, and W. Emery (2007), A younger, thinner Arctic ice cover: Increased potential for rapid, extensive sea-ice loss, *Geophys. Res. Lett.*, *34*, L24501, doi:10.1029/2007GL032043.

Maslanik, J. A., J. Stroeve, C. Fowler, and W. Emery (2011), Distribution and trends in Arctic sea ice age through spring 2011, *Geophys. Res. Lett.*, *38*, L13502, doi:10.1029/2011GL047735.

Mauritsen, T., et al. (2012), Tuning the climate of a global model, *J. Adv. Model. Earth Syst.*, *4*, M00A01, doi:10.1029/2012MS000154.

Meehl, G. A., et al. (2007), Global climate projections, in *Climate Change 2007: The Physical Science Basis. Contribution of Working Group I to the Fourth Assessment Report of the Intergovernmental Panel on Climate Change*, edited by S. Solomon et al., pp. 747–845, Cambridge Univ. Press, Cambridge, U. K.

Moss, R. H., et al. (2010), The next generation of scenarios for climate change research and assessment, *Nature*, *463*, 747–756, doi:10.1038/nature08823.

Nghiem, S. V., I. G. Rigor, D. K. Perovich, P. Clemente-Colón, J. W. Weatherly, and G. Neumann (2007), Rapid reduction of Arctic perennial sea ice, *Geophys. Res. Lett.*, *34*, L19504, doi:10.1029/2007GL031138.

Pedersen, C. A., E. Roeckner, M. Lüthje, and J.-G. Winther (2009), A new sea ice albedo scheme including melt ponds for ECHAM5 general circulation model, *J. Geophys. Res.*, *114*, D08101, doi:10.1029/2008JD010440.

Perovich, D. K., T. C. Grenfell, B. Light, and P. V. Hobbs (2002a), Seasonal evolution of the albedo of multiyear Arctic sea ice, *J. Geophys. Res.*, *107*(C10), 8044, doi:10.1029/2000JC000438.

Perovich, D. K., W. B. Tucker III, and K. A. Ligett (2002b), Aerial observations of the evolution of ice surface conditions during summer, *J. Geophys. Res.*, *107*(C10), 8048, doi:10.1029/2000JC000449.

Perovich, D. K., T. C. Grenfell, B. Light, B. C. Elder, J. Harbeck, C. Polashenski, W. B. Tucker III, and C. Stelmach (2009), Transpolar observations of the morphological properties of Arctic sea ice, *J. Geophys. Res.*, *114*, C00A04, doi:10.1029/2008JC004892.

Polashenski, C., D. Perovich, and Z. Courville (2012), The mechanisms of sea ice melt pond formation and evolution, *J. Geophys. Res.*, *117*, C01001, doi:10.1029/2011JC007231.

Rampal, P., J. Weiss, C. Dubois, and J.-M. Campin (2011), IPCC climate models do not capture Arctic sea ice drift acceleration: Consequences in terms of projected sea ice thinning and decline, *J. Geophys. Res.*, *116*, C00D07, doi:10.1029/2011JC007110.

Rigor, I. G., and J. M. Wallace (2004), Variations in the age of Arctic sea-ice and summer sea-ice extent, *Geophys. Res. Lett.*, *31*, L09401, doi:10.1029/2004GL019492.

Sankelo, P., J. Haapala, I. Heiler, and E. Rinne (2010), Melt pond formation and temporal evolution at the drifting station Tara during summer 2007, *Polar Res.*, *29*, 311–321, doi:10.1111/j.1751-8369.2010.00161.x.

Stroeve, J., M. M. Holland, W. Meier, T. Scambos, and M. Serreze (2007), Arctic sea ice decline: Faster than forecast, *Geophys. Res. Lett.*, *34*, L09501, doi:10.1029/2007GL029703.

Tschudi, M. A., J. A. Curry, and J. A. Maslanik (2001), Airborne observations of summertime surface features and their effect on surface albedo during FIRE/SHEBA, *J. Geophys. Res.*, *106*(D14), 15,335–15,344, doi:10.1029/2000JD900275.

Tschudi, M. A., J. A. Maslanik, and D. K. Perovich (2008), Derivation of melt pond coverage on Arctic sea ice during MODIS observations, *Remote Sens. Environ.*, *112*, 2605–2614, doi:10.1016/j.rse.2007.12.009.

Tucker, W. B., III, A. J. Grow, D. A. Meese and H. W. Bosworth (1999), Physical characteristics of summer sea ice across the Arctic Ocean, *J. Geophys. Res.*, *104*, 1489–1504, doi:10.1029/98JC02607.

Winton, M. (2011), Do climate models underestimate the sensitivity of Northern Hemisphere sea ice cover? *J. Clim.*, *24*, 3924–3934, doi:10.1175/2011JCLI4146.1.

Yackel, J. J., D. G. Barber, and J. M. Hanesiak (2000), Melt ponds on sea ice in the Canadian Arctic Archipelago: Part 1. Variability in morphological and radiative properties, *J. Geophys. Res.*, *105*(C9), 22,049–22,060, doi:10.1029/2000JC900075.

Corresponding author: E. Roeckner, Max Planck Institute for Meteorology, Bundesstrasse 53, D-20146 Hamburg. Germany. (erich.roeckner@zmaw.de)